Concurrent quantum eigensolver for multiple low-energy eigenstates

G. Xu,[1,*] Y. B. Guo,[1,2,*] X. Li,[1,2] K. Wang,[1,2] Z. Fan,[1,2] Z. S. Zhou,[1] H. J. Liao,[1,3,†] and T. Xiang[1,2,4,‡]

[1]*Institute of Physics, Chinese Academy of Sciences, Beijing 100190, China*

[2]*School of Physical Sciences, University of Chinese Academy of Sciences, Beijing 100049, China*

[3]*Songshan Lake Materials Laboratory, Dongguan, Guangdong 523808, China*

[4]*Beijing Academy of Quantum Information Sciences, Beijing 100190, China*

(Received 25 November 2022; revised 28 April 2023; accepted 10 May 2023; published 30 May 2023)

We propose a quantum algorithm that diagonalizes a Hamiltonian by implementing an ansatz that satisfies the generalized Rayleigh-Ritz variational principle. This algorithm uses a purification technique to target many quantum states in one quantum circuit and allows multiple eigenstates to be optimized and determined simultaneously. Moreover, it requires a reasonable circuit depth compared to existing algorithms and enables flexible postprocessing on the accurately determined eigensubspace. Using the transverse-field Ising model, we confirm that the eigenvalues obtained with the algorithm converge efficiently and uniformly with the iteration steps, tested by both simulations and IBM platform measurements. As limited quantum resources are needed, this algorithm is promising for noise resilience, better performances, and versatile applications.

DOI: 10.1103/PhysRevA.107.052423

I. INTRODUCTION

Quantum computations and simulations utilize quantum devices to solve classical or quantum problems and hold promise for tackling large-scale systems that are intractable with conventional computers. For example, several quantum algorithms have demonstrated the potential to show exponential or quadratic speedup over their classical counterparts [1–4]. Their implementation has stimulated surging interest in the exploration of quantum computing devices [5,6], such as superconducting circuits [7], ultracold atoms [8], trapped ion systems [9], photonic systems [10], and systems of nuclear magnetic resonance with nitrogen-vacancy spins [11].

Quantum computing has advanced into the noisy intermediate-scale quantum (NISQ) era [12,13]. Successful manipulations of quantum circuits with more than 50 qubits have demonstrated the so-called quantum supremacy [14–17]. However, the current quantum processors cannot conduct large-scale fault-tolerant quantum computation. In particular, the limited coherence time of qubits, environmental noises, and the connectivity of NISQ devices put strong constraints on the scale of applications of quantum algorithms. Nevertheless, NISQ devices are valuable tools for exploring many-body quantum physics and other fields and represent a significant step toward more powerful quantum technologies in the future.

In recent years, several variational quantum algorithms (VQAs) [18] were proposed to solve classical or quantum problems by parametrizing quantum circuits using classical-quantum hybrid optimization schemes. This has led to, for example, successful applications of NISQ devices in combinatorial optimization and adiabatic quantum computation [19,20], quantum chemistry [21–30], machine learning [31–34], and condensed-matter physics [35–42]. A particular successful algorithm is the variational quantum eigensolver (VQE) [21,43]. It is one of the earliest VQAs introduced for solving ground states using NISQ computers [19–27,31,32].

The VQE has also been extended to determine excited eigenstates of a Hamiltonian [22,28–30,42,44–49]. However, the extension has encountered severe challenges imposed by the limited coherence time of qubits. First, it is much more sensitive and hard to prepare an initial state orthogonal to the ground state without intensively increasing quantum resources. Second, with the increase of the number of diagonalized eigenstates, the algorithms require more quantum resources such as deeper quantum circuits for more variational parameters or several quantum circuits for calculating different terms in optimization functions. Third, the solution relies highly on the performance of quantum hardware. One of the main error resources is the readout error from the manufacture of NISQ devices. The readout error will inevitably introduce additional uncertainty in determining a targeted eigenstate as accurately as the ground state. For example, the orthogonality-constrained VQE [45] and the variational-quantum-deflation algorithm [46,47] solve the eigenstates recursively but suffer from accumulative errors and extra quantum resource demands. The subspace-search VQE (SSVQE) [48] requires an additional optimization process to yield an accurate approximation for a specific excited state which has to increase the circuit depth as a penalty. A variant of SSVQE that assigns different weights of searched states could eliminate additional optimizations. This weighted SSVQE possesses different degrees of accuracy as the loss function is more insensitive to lower-weighted trial states, which results in higher-energy eigenstates suffering larger optimization errors.

*These authors contributed equally to this work

†Corresponding author: navyphysics@iphy.ac.cn

‡Corresponding author: txiang@iphy.ac.cn

The multistate-contracted VQE [49], on the other hand, can solve some eigenstates for some specific Hamiltonians simultaneously but still has difficulty in preparing the initial states.

In this article, we propose a variational quantum algorithm to optimize the ground and excited states concurrently using a purification technique by introducing ancillary qubits (called ancillas). The steps for implementing this algorithm are almost the same as for VQE. Nevertheless, it resolves all the difficulties mentioned above. First, the circuit can be initialized simply by pairing each ancilla with a physical qubit to form a maximally entangled state (i.e., a Bell state). It is simple to carry out this initialization step in the currently available quantum computers. Second, the variational parametrization of the circuit applies only to the physical qubits without involving the ancillary qubits, greatly simplifying the circuit design. It requires quantum resources comparable to those of existing algorithms, allowing us to target many eigenstates simultaneously. Third, the algorithm enables us to measure the matrix elements between any two targeted eigenstates simply by manipulating the ancilla states. This measurement protocol significantly reduces the readout errors without adding more circuit layers. As all targeted eigenstates are determined using the same quantum circuit, they should converge uniformly (namely, have the same order of accuracy). Hence, our algorithm has great potential for practical applications of quantum processors against noisy implementations.

II. CONCURRENT QUANTUM EIGENSOLVER

The VQE uses a quantum circuit to parametrize the ground state of a Hamiltonian variationally. Using gradient descendant optimization processes [50,51], the VQE has demonstrated great potential on NISQ devices. However, this quantum algorithm cannot be used to simultaneously find a set of eigenstates, say, the K lowest-energy eigenstates, because a VQE circuit cannot accommodate two or more orthogonal trial states at one time. To resolve this difficulty, we introduce a set of ancillas to convert K orthogonal trial states into a pure quantum state. This procedure is known as "purification" in quantum information. The optimization can then be imposed on this purified quantum state using only one quantum circuit. Our algorithm is able to tune the weights of different trial states on the hardware and realizes the weighted SSVQE [48]. Nevertheless, we choose uniformly weighted trial states to achieve the determination of eigenstates with the same degree of optimization accuracy. This key feature is extremely helpful in the determination of transition energies in quantum chemistry and the mass spectrum of the massive Schwinger model in high-energy physics [52–54], for instance.

Purification of quantum states by introducing ancillas is a common practice used in physics [55], particularly in the study of the thermodynamics of quantum many-body systems [56,57] and in quantum computation [58,59]. This technique has also been applied to investigate dynamical Green's functions through variationally optimized quantum circuits [59]. Furthermore, as demonstrated below, the use of this technique in our algorithm significantly reduces the complexity and depth of the quantum circuit compared to algorithms that change Hamiltonians or loss functions during determinations of serial eigenstates. Later, we will analyze the measurement requirements of our algorithm, which potentially reduces the effects of readout errors or the quantum resources of error-mitigation methods.

Let us consider a system of N_p physical qubits (we call it a physical system) on which the Hamiltonian $\hat{H}$ is embedded. In order to determine the K lowest-energy eigenstates, we first introduce N_a ancillary qubits to construct a purified quantum state from which K orthogonal trial states can be optimized. Here N_a should be larger than or equal to $\log_2 K$ but smaller than N_p. The whole system, therefore, contains N_p physical qubits and N_a ancillas. The variational optimization of this purified quantum state is carried out by performing unitary transformations for only the physical qubits. As a result, the ancilla states are not altered by the circuit once initialized, ensuring the orthogonality remains throughout the calculation. This process is widely used to embed the desired mixed-state density matrix using ancillary qubits [60–62]. However, previous algorithms [48,60] achieved the same purpose of cost-function embedding using classical samplings of different initial states with the same quantum resources consumption. In addition, because the loss function is irrelevant to the ancillary qubits states, trace-preserving quantum noise on ancillas would not affect the optimization process. The training process does not require measurement information from the ancillary qubits. Therefore, our algorithm requires only a total number of measurements $N_{\text{meas}} \propto N_p$ per optimization step.

We initialize the system by demanding that the physical qubits form a maximally entangled state with the N_a ancillas,

$$|\psi_{\text{init}}\rangle = \frac{1}{\sqrt{M}} \sum_{\alpha=0}^{M-1} |\alpha\rangle^p \otimes |\alpha\rangle^a \quad (M = 2^{N_a}), \tag{1}$$

where $\{|\alpha\rangle^p\}$ and $\{|\alpha\rangle^a\}$ are the M orthogonal basis states of the physical and ancillary systems, respectively. For the ancillary system, the orthogonal basis states can be simply taken as product states of local bases $\{|0\rangle^a, |1\rangle^a\}$. This maximally entangled state can be readily prepared by requiring, for example, each of the first N_a qubits in the physical system to form a maximally entangled state with a corresponding ancilla, and the rest of the physical qubits are all in the up-spin states, namely,

$$|\psi_{\text{init}}\rangle = \bigotimes_{i=1}^{N_a} |B\rangle_i \bigotimes_{j=N_a+1}^{N_p} |0\rangle_j^p, \tag{2}$$

where $|B\rangle_i$ is a Bell state formed by the ith physical qubit and the ith ancilla [58], $|B\rangle_i = 1/\sqrt{2}(|0\rangle^p|0\rangle^a + |1\rangle^p|1\rangle^a)_i$. Of course, one can also choose other N_a qubits from the physical system to form a maximally entangled state with the ancillas.

The variational wave function is defined by applying a unitary operation $U(\theta) \otimes \mathbb{I}^a$ to the initial state,

$$|\psi(\theta)\rangle = U(\theta) \otimes \mathbb{I}^a |\psi_{\text{init}}\rangle, \tag{3}$$

where $\mathbb{I}^a$ represents identity operators on ancillary qubits, $U(\theta)$ acts on only the physical qubits, and θ are the variational parameters. It is parameterized as a quantum circuit $U(\theta) = \prod_{l=1}^{L} U_l(\theta_l), \quad \theta = (\theta_1, \ldots, \theta_L)$, where $U_l(\theta_l)$ is a unitary operator that acts on the lth layer of the circuit and

θ_l is a collection of all variational parameters in that layer. In general, the depth of the designed ansatz should be deliberately balanced for overall performance, considering the size of the searching Hilbert space and avoiding the barren plateau phenomenon [63]. In practice, quantum hardware limitations, such as the connectivity of the architecture, the quantum noise of unitary gates, and the coherent time of reliable qubits, should also be evaluated.

The loss function we used is the total energy expectation value of K orthogonal physical states, which can be selected from the first K ancillary states upon measurements [48,49]

$$\mathcal{L}(\theta) = \sum_{\alpha=0}^{K-1} {}^{p}\langle\bar{\alpha}|\hat{H}|\bar{\alpha}\rangle^{p}, \tag{4}$$

where $|\bar{\alpha}\rangle^p = U(\theta)|\alpha\rangle^p$ is the final state of the physical qubits. This loss function, according to the generalized Rayleigh-Ritz variational principle [64], sets an upper bound on the sum of the K lowest eigenvalues $(E_0, \ldots, E_{K-1})$, of $\hat{H}$, i.e.,

$$\mathcal{L}(\theta) \geqslant \sum_{i=0}^{K-1} E_i. \tag{5}$$

The eigenvalues are assumed to be ascending ordered, $E_0 \leqslant E_1 \leqslant \cdots \leqslant E_{K-1}$. E_0 is the ground-state energy. To determine the K lowest eigenvalues and the corresponding eigenvectors of $\hat{H}$, we minimize the loss function by variationally optimizing all the gate parameters θ.

III. DETERMINATION OF LOW-ENERGY EIGENSPECTRA

After minimizing the loss function, we evolve the physical qubits onto the subspace spanned by the K lowest-energy states of $\hat{H}$. However, for a given ancillary state $|\alpha\rangle^a$, the corresponding physical state $|\bar{\alpha}\rangle^p$ generated by the circuit is not automatically an eigenstate of $\hat{H}$. This is because the loss function depends on the sum of the energy expectation values of the K lowest eigenstates and cannot distinguish any unitary rotations of these states in that basis subspace. For instance, we note a unitary rotation in the target eigensubspace $\tilde{U} = \sum_{ij} \tilde{U}_{ij}|E_i\rangle\langle E_j|$, and the reduced density matrix of trained states on physical qubits is $\rho = M^{-1}\sum|\psi_l\rangle\langle\psi_l|$. Given the commutation relation between U and H, $[U, H] = 0$, the loss function is $\mathrm{Tr}(H\rho) = \mathrm{Tr}(\tilde{U}^\dagger\tilde{U}H\rho) = \mathrm{Tr}(H\tilde{U}\rho\tilde{U}^\dagger) \equiv \mathrm{Tr}(H\tilde{\rho})$. In this case, the ansatz cannot distinguish $\tilde{\rho}$ and ρ in the training process. The output trained states can be any possible states $\tilde{U}|\psi_l\rangle$ other than $|\psi_l\rangle$. On the other hand, if we acquired information on the matrix representation of H in the basis of trained states, we would be able to eliminate the possible rotations by diagonalization of this matrix.

Thus, we need to determine the energy eigenstates through measurements of not only the diagonal matrix elements of $\hat{H}$, i.e., ${}^{p}\langle\bar{\alpha}|\hat{H}|\bar{\alpha}\rangle^{p}$, but also all off-diagonal matrix elements, i.e., $H_{\beta,\alpha} \equiv {}^{p}\langle\bar{\beta}|\hat{H}|\bar{\alpha}\rangle^{p}$ $(\beta \neq \alpha)$ in the final states.

To measure the off-diagonal matrix elements of $\hat{H}$, generally, one has to take a unitary transformation to construct a superposition of physical states $|\bar{\alpha}\rangle^p$ and $|\bar{\beta}\rangle^p$. In conventional algorithms, it is difficult to determine the transformation and perform corresponding rotations [49]. In our algorithm, however, as the ancillas are maximally entangled with the physical qubits, we can implement this unitary transformation effectively by rotating only the ancillary qubits. In other words, to change the physical state from $|\bar{\alpha}\rangle^p$ to $|\bar{\beta}\rangle^p$, we just need to change the corresponding ancillary state from $|\alpha\rangle^a$ to $|\beta\rangle^a$. This basis transformation or rotation does not alter the quantum states of the physical qubits. It provides a feasible scheme to retrieve interesting physical quantities that are difficult to measure directly.

TABLE I. Example of measuring the outcome to determine the energy expectation matrix. The operators $|i\rangle\langle j|$ are applied on the ancillary qubits.

Observables	Operators	Expectation values
$\hat{H}\otimes(I+Z)/2$	$\hat{H}\otimes\|0\rangle\langle 0\|$	H_{00}
$\hat{H}\otimes(X+iY)/2$	$\hat{H}\otimes\|0\rangle\langle 1\|$	H_{01}
$\hat{H}\otimes(X-iY)/2$	$\hat{H}\otimes\|1\rangle\langle 0\|$	H_{10}
$\hat{H}\otimes(I-Z)/2$	$\hat{H}\otimes\|1\rangle\langle 1\|$	H_{11}

In some cases, we use N_a ancillary qubits to determine $M = 2^{N_a}$ eigenstates which might exceed the number of target eigenstates, K, i.e., $M \geqslant K$. It is simple to show that the expectation value of the operator $\hat{H}\otimes|\beta\rangle^a\langle\alpha|$ in the final state $|\psi(\theta)\rangle$ equals the matrix element of the Hamiltonian,

$$H_{\beta,\alpha} = M\langle\psi(\theta)|\big(\hat{H}\otimes|\beta\rangle^a\langle\alpha|\big)|\psi(\theta)\rangle. \tag{6}$$

For each element of the Hamiltonian $H_{\beta,\alpha}$, it can be "labeled" by the ancillary operator $|\beta\rangle^a\langle\alpha|$. By calculating the linear combination of Pauli operators of the position label, we obtain the corresponding observables on the ancillas. For example, we calculate H_{00} by evaluating the expectation value of $\hat{H}\otimes|0\rangle^a\langle 0|$, and the linear combination for the observable on the ancillas is $|0\rangle^a\langle 0| = (I+Z)/2$. Here we demonstrate the elements of the Hamiltonian and corresponding observables for the case with one ancillary qubit in Table I. Refer to the Appendix for general cases.

We note the diagonalization of $H_{\beta,\alpha}$ with a unitary matrix S,

$$H_{\beta,\alpha} = \sum_{i=0}^{M-1} S_{\beta,i}E_iS^*_{\alpha,i}; \tag{7}$$

thus, we obtain all the eigenvalues and eigenvectors. If the eigenvalues are ascending ordered, then the first K eigenvalues E_i $(i = 0, \ldots, K-1)$ are what we hope to target. The corresponding eigenstates are given by

$$|E_i\rangle^p = \sum_{\alpha=0}^{M-1} S_{\alpha,i}|\bar{\alpha}\rangle^p. \tag{8}$$

This determination of matrix elements is conducted after the convergence of the loss function, and the number of searched states during the optimization process is M $(\geqslant K)$, which is similar to those in SSVQE or other existing methods. The above scheme also allows us to measure the expectation value of a physical operator, such as the thermal average, by taking actions on the ancillary qubits. Refer to the Appendix for more details.

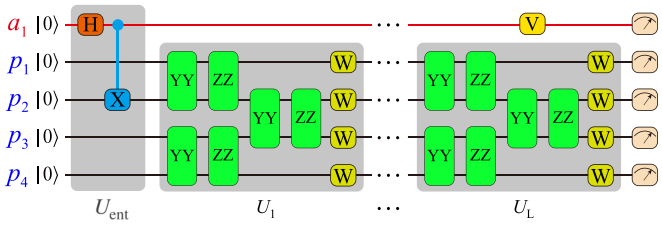

FIG. 1. Sketch of a quantum circuit for implementing a variational optimization for $N_p = 4$ and $N_a = 1$ systems. An entanglement generator U_{ent} is applied between the ancillary and physical qubits to prepare a purified initial state. U_l is a collection of all unitary gate operations, which act only on physical qubits, in the lth layer of the circuit. H is the Hadamard gate. V denotes a postprocessing operator, which applies to the ancillas only.

IV. RESULTS

As an application and demonstration, we apply our method to the one-dimensional quantum transverse-field Ising model (TFIM),

$$\hat{H} = -J \sum_i S_i^z S_{i+1}^z + h_x \sum_i S_i^x, \tag{9}$$

where S_i^x and S_i^z are the $S = 1/2$ spin operators. This model is exactly soluble, allowing us to compare the results obtained with simulations using our algorithm with the exact ones. We do the calculation at the point $h_x = 0.5$ and $J = 1$, where the ground state of this model becomes critical in the thermodynamic limit.

Figure 1 shows an example of the trial states prepared for a system of $N_p = 4$ and $N_a = 1$. In this case, the ancillary qubit is maximally entangled with the physical qubit labeled by p_2 in the initial state. Each layer of the variational ansatz can be represented as [38,65] $U_l(\theta_l) = W(\theta_l) R_{ZZ}(\theta_{l,2}) R_{YY}(\theta_{l,1})$, where W represents the product of three single-qubit rotation gates, $W(\theta_l) = R_X(\theta_{l,5}) R_Z(\theta_{l,4}) R_X(\theta_{l,3})$, and (X, Y, Z) represent the three Pauli matrices $(\sigma_x, \sigma_y, \sigma_z)$. R_Q is a rotation gate along the Q axis, $R_Q(\theta) = \exp(i\theta Q/2)$. Each layer comprises two sublayers of two-qubit gates, R_{YY} and R_{ZZ}, in a brick-wall structure and three sublayers of single-qubit gates, R_X, R_Z, and R_X. Each unitary gate is parameterized by one variational parameter.

Let us first solve the four lowest eigenstates in an eight-spin system. Figure 2(a) shows how the four eigenvalues E_i $(i = 0, \ldots, 3)$ vary with the optimization step m for TFIM. The four eigenvalues converge very quickly with the increase of m. Their differences from the exact eigenvalues E_i^{ex}, $\delta E_i = E_i - E_i^{\text{ex}}$, drop exponentially at nearly the same speed as m for all the eigenvalues [Fig. 2(b)]. Hence, the four eigenvalues uniformly converge—the absolute errors of the converging eigenvalues are of the same order of magnitude. This implies that the energy differences between any two eigenvalues evaluated are more accurate than the eigenvalues themselves. This is, indeed, what we see, for example, by comparing the error of the energy difference $\delta\Delta_1 = |\delta E_1 - \delta E_0|$ with the errors of E_1 and E_0, as shown in Fig. 2(c).

However, it should be noted that the eigenstates obtained with the circuit shown in Fig. 1 may not always be the K lowest ones. For example, if we still use that circuit to calculate eight eigenstates using three ancillas, we find that

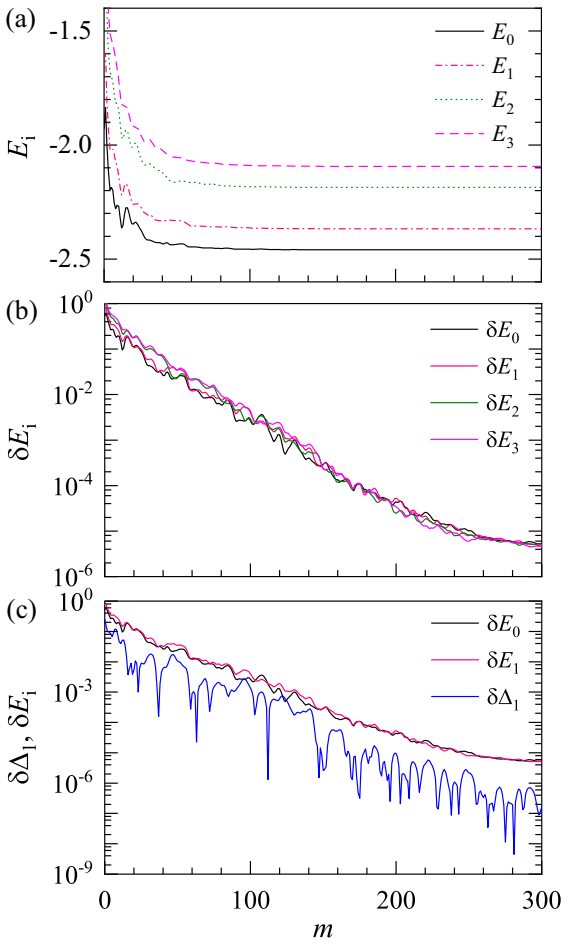

FIG. 2. Four lowest eigenvalues obtained with a purified trial wave function using two ancillas for the eight-spin transverse Ising model with $h_x = 0.5$ and $J = 1$. The energy values plotted are in units of J. (a) shows the four lowest eigenvalues, E_0 (solid line), E_1 (dash-dotted line), E_2 (dotted line), and E_3 (dashed line), and (b) shows how their absolute errors converge with the iteration number of optimizations m. (c) Comparison between the error of the spectral gap $\delta\Delta_1$ (lower line) and the errors of E_0 and E_1.

six of them are, indeed, the lowest eigenvalues of the system. Still, the other two converge to the eighth and tenth excited eigenvalues, respectively. Hence, the sixth and seventh excited eigenstates are missing due to some restriction imposed by $U(\theta)$ on the variational subspace, which prohibits these two eigenstates from being targeted by the circuit. There are two ways to solve this problem. One is to increase the number of ancillas. For example, by expanding the number of ancillas from three to four, we can correctly obtain the eight lowest eigenvalues, still using that circuit. The other is redesigning the unitary circuit $U(\theta)$ to avoid trapping the targeted states in some restricted subspace. A detailed discussion of this issue is given in the Appendix.

We further examine the algorithm by calculating the two lowest eigenvalues of TFIM using the Oslo quantum processor on the IBM quantum computing platform. This is a direct test of the algorithm on a NISQ computer. To avoid using too many two-qubit gates in a circuit (which have relatively large implementation errors), we modify the variational ansatz. The

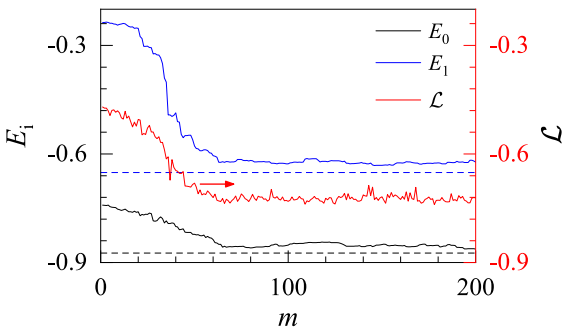

FIG. 3. The ground-state energy E_0 (lower line), the first excited eigenenergy E_1 (upper line), and the loss function $\mathcal{L}$ (middle line) obtained with a purified trial wave function using one ancilla for the three-spin TFIM with $h_x = 0.5$ and $J = 1$. The energy values plotted are in units of J. The relative errors of the ground and first excited eigenenergies are 1.244% and 2.924% compared to the exact results (dashed horizontal lines), respectively.

revised circuit design is shown in Fig. 6 in the Appendix. As the quantum computing resources publicly available are limited, we demonstrate the method using only four qubits, which contain three physical qubits and one ancilla. Figure 3 shows the output after 200 iterations: both the ground and first excited eigenenergies converge quickly with the iteration number. Their relative errors are 1.244% and 2.924% compared to the exact ones. The corresponding relative error in the loss function is ∼2.971%. Refer to the Appendix for more technical details of this test.

V. SUMMARY

We have proposed a quantum algorithm for concurrently optimizing multiple low-energy eigenstates of a Hamiltonian using a quantum circuit. This algorithm resolves all the major problems in the determination of these eigenstates by parametrizing a quantum circuit variationally. It is resilient to noisy implementations on NISQ hardware and can be implemented as efficiently as the standard VQE. Furthermore, it can access all the matrix elements (including the off-diagonal ones) of the Hamiltonian or other physical observables simply by manipulating ancillary states, significantly reducing the readout error without increasing the circuit depth.

Our algorithm does not increase the requirement of the hardware connectivity significantly, which is mainly due to the purification module. Potentially, our algorithm is applicable on sparsely connected two-dimensional quantum hardware. For instance, the algorithm can be readily implemented on a NISQ device with a ladder-shaped architecture [14–16]. We have tested the algorithm on a NISQ computer by taking TFIM as an example. Our test, although still on a relatively small-scale quantum computing platform, does show the promise of our algorithm for low-energy eigenspectra calculations on upcoming large-scale NISQ and fault-tolerant quantum computers.

ACKNOWLEDGMENTS

This work is supported by the National Key Research and Development Project of China (Grants No. 2017YFA0302901 and No. 2022YFA1403900), the National Natural Science Foundation of China (Grants No. 11888101 and No. 11874095), the Youth Innovation Promotion Association of CAS (Grant No. 2021004), and the Strategic Priority Research Program of the Chinese Academy of Sciences (Grants No. XDB33010100 and No. XDB33020300).

APPENDIX

1. Determination of low-energy eigenspectra

The basis transformation from $|\alpha\rangle^a$ to $|\beta\rangle^a$ can be achieved by applying the operator $|\beta\rangle^a\langle\alpha|$ to the ancillary system. For each ancilla, say the ith one, this basis transformation operator takes four possible values, $|\beta_i\rangle\langle\alpha_i| = (|0\rangle\langle 0|, |0\rangle\langle 1|, |1\rangle\langle 0|, |1\rangle\langle 1|)_i$, depending on the initial and final basis states of the ancilla. These four basis transformation operators are related to the four unitary operators, $\hat{A}^i = (I, \sigma_x, \sigma_y, \sigma_z)_i$, by the transformation

$$|\beta_i\rangle\langle\alpha_i| = \sum_{\mu_i} v_{\beta_i\alpha_i,\mu_i}\hat{A}^i_{\mu_i}, \tag{A1}$$

where I is the identity matrix, $(\sigma_x, \sigma_y, \sigma_z)$ are the three Pauli matrices, and v is a 4×4 matrix if we regard $(\beta_i\alpha_i)$ as one index,

$$v = \frac{1}{2}\begin{pmatrix} 1 & 0 & 0 & 1 \\ 0 & 1 & i & 0 \\ 0 & 1 & -i & 0 \\ 1 & 0 & 0 & -1 \end{pmatrix}. \tag{A2}$$

It is simple to show that the expectation value of the operator $\hat{H}\otimes|\beta\rangle^a\langle\alpha|$ in the final state $|\psi(\theta)\rangle$ equals the matrix element of the Hamiltonian,

$$\begin{aligned} H_{\beta,\alpha} &\equiv {}^p\langle\bar{\beta}|\hat{H}|\bar{\alpha}\rangle^p \\ &= M\langle\psi(\theta)|(\hat{H}\otimes|\beta\rangle^a\langle\alpha|)|\psi(\theta)\rangle. \end{aligned} \tag{A3}$$

Substituting (A1) into the above equation, we find that

$$H_{\beta,\alpha} = M\sum_{\mu} V_{\beta\alpha,\mu}\langle\psi(\theta)|\hat{H}\otimes\hat{A}_\mu|\psi(\theta)\rangle, \tag{A4}$$

where

$$\hat{A}_\mu = \prod_{i=1}^{N_a}\otimes\hat{A}^i_{\mu_i}, \quad \mu = (\mu_1, \ldots, \mu_{N_a}), \tag{A5}$$

$$V_{\beta\alpha,\mu} = \prod_{i=1}^{N_a} v_{\beta_i\alpha_i,\mu_i}, \quad \beta = (\beta_1, \ldots, \beta_{N_a}). \tag{A6}$$

Equation (A4) indicates that by measuring the expectation values of the operators $\hat{H}\otimes\hat{A}_\mu$ (the total number of these operators is 4^{N_a}) in the state $|\psi(\theta)\rangle$,

$$h_\mu = \langle\psi(\theta)|\hat{H}\otimes\hat{A}_\mu|\psi(\theta)\rangle, \tag{A7}$$

we can obtain the matrix element of the Hamiltonian,

$$H_{\beta,\alpha} = M\sum_{\mu} V_{\beta\alpha,\mu}h_\mu. \tag{A8}$$

The above scheme allows us to measure the expectation value of a physical operator simply by rotating the ancillary states. As an example, let us calculate the thermal average of a

physical observable $\hat{O}$ in the physical subspace spanned by the previously determined eigenstates of $\hat{H}$,

$$\langle \hat{O} \rangle = \mathrm{Tr}(\rho \hat{O}), \tag{A9}$$

$$\rho = Z^{-1} \sum_i e^{-\beta E_i} |E_i\rangle^p \langle E_i|, \tag{A10}$$

where $Z = \sum_i e^{-\beta E_i}$ is an approximate partition function and β is the inverse temperature. Again, it is difficult to determine this quantity just by measuring the states of the physical qubits. To solve this problem, we introduce a diagonal Hermitian operator in the ancillary system,

$$\hat{T} = Z^{-1} \sum_i e^{-\beta E_i} |E_i\rangle^a \langle E_i|, \tag{A11}$$

where

$$|E_i\rangle^a = \sum_{\alpha=0}^{M-1} S_{\alpha,i} |\alpha\rangle^a. \tag{A12}$$

It is straightforward to show that

$$\langle \hat{O} \rangle = M \langle \psi(\theta)| \hat{O} \otimes \hat{T} |\psi(\theta)\rangle. \tag{A13}$$

Hence, the thermal average of $\hat{O}$ can be obtained just by measuring the expectation value of $\hat{O} \otimes \hat{T}$ on the final state.

2. Simulation of the transverse-field Ising model

a. Determination of four lowest eigenstates

As an application example of our algorithm, let us first solve the four lowest eigenstates in an eight-spin system. The dimension of the full Hamiltonian is 256. We use two ancillas to purify the quantum state. The variational parameters θ in the ansatz defined by Fig. 1 in the main text are randomly initialized within an interval $[0, 0.1)$. The optimization is iteratively conducted a few hundred times until all the variational parameters converge. This optimization step is taken 21 times, starting from different initial variational parameters. We use the best set of parameters that minimizes the loss function to evaluate the four lowest eigenpairs of the Hamiltonian.

To determine the matrix elements of the Hamiltonian with four eigenstates, we first evaluate the expectation values h_μ of the $4^2 = 16$ operators $\hat{H} \otimes \hat{A}_\mu$ defined in Eq. (A7). Substituting the results into Eq. (A8), we then obtain all the 4×4 matrix elements of $\hat{H}$ in the optimized basis subspace. The four lowest eigenvalues are obtained by diagonalizing this 4×4 matrix. The results are shown in Fig. 2 in the main text.

b. Determination of eight lowest eigenstates

In a circuit with N_a spins, up to 2^{N_a} eigenstates can be simultaneously optimized with our algorithm. However, these eigenstates may not be the lowest-energy ones for a given unitary operator $U(\theta)$ because, in some cases, $U(\theta)$ can access only part of the Hilbert subspace spanned by the 2^{N_a} lowest eigenstates. As shown in Fig. 4, this is, indeed, what we see in the variational calculation for the eight lowest eigenvalues of the eight-spin TFIM using the unitary ansatz shown in Fig. 1 in the main text with three ancillas. For comparison, we also show the exact results for the lowest 11 eigenvalues of the same system in the right panel of Fig. 4. Among the eight

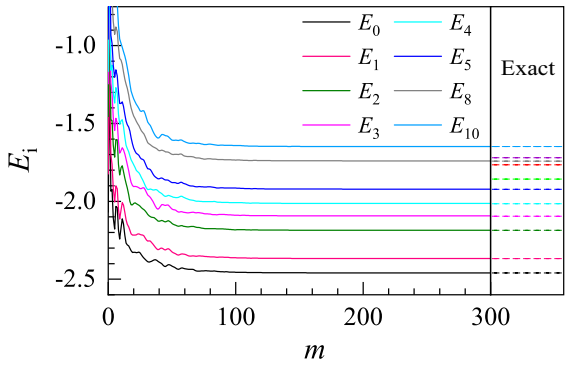

FIG. 4. Eight low-energy eigenvalues obtained using three ancillas for the eight-spin TFIM. The left panel shows how the eight eigenvalues converge with the optimization step m. The right panel shows the lowest 11 eigenvalues in ascending order from the bottom obtained by exact diagonalization. Among these 11 eigenvalues, the sixth, seventh, and ninth excited eigenvalues are skipped in the variational calculation. Six variational layers ($L = 6$) are used.

eigenvalues we obtain, six of them, including the ground-state energy and the energies of the five lowest excited eigenstates, converge to the exact results. The other two eigenvalues, however, converge to the eighth and tenth excited eigenvalues. Hence, the sixth and seventh excited eigenstates are missing in the variational calculation.

To understand why the variational optimization does not produce the eight lowest eigenstates, we evaluate the wave function overlaps between the true eight lowest eigenstates of the Hamiltonian and the eight optimized basis states $|\bar{\alpha}\rangle^p$ ($\alpha = 0, \ldots, 7$),

$$M_{i,\alpha} = \left\langle E_i^{\mathrm{ex}} \middle| \bar{\alpha} \right\rangle^p. \tag{A14}$$

In order to obtain all the eight lowest-energy eigenstates of $\hat{H}$, M should be a matrix of rank 8. However, in our calculation, we find that its rank is 6, indicating that only six out of the eight lowest-energy eigenstates of $\hat{H}$ can be obtained from the variational ansatz we adopt if three ancillary qubits are used.

If the variational ansatz is not changed in our layered circuit structures, one way to solve the above problem is to increase the number of ancillas. By introducing more ancillary qubits, we are able to optimize the wave function in a larger Hilbert subspace. By increasing the number of ancillas, we should be able to find the eight lowest eigenpairs. In other words, if the eigenpairs so obtained do not change with the increase of the number of ancillas, they should be the targeted eight lowest eigenpairs.

For the eight-spin TFIM, we find that it is sufficient to find the eight lowest-energy eigenstates by utilizing four ancillas. Figure 5(a) shows how the eight lowest eigenvalues of $\hat{H}$ converge with the iteration step m. The absolute errors δE_i ($i = 0, \ldots, 7$) of these eigenvalues, shown in Fig. 5(b), drop exponentially and uniformly with m. For all eight eigenvalues, the errors become less than 10^{-6} if six layers ($L = 6$) are used and m becomes larger than 300. The errors can be further reduced if more iteration steps are taken to optimize the variational parameters.

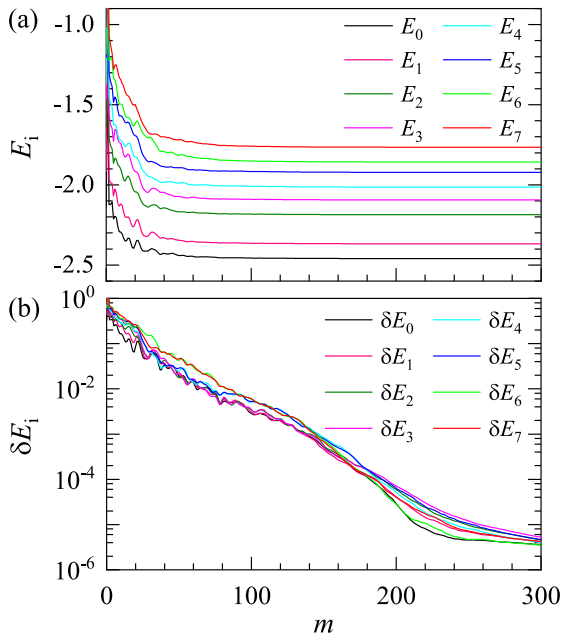

FIG. 5. Eight lowest eigenvalues obtained in ascending order from the bottom using four ancillas for the eight-spin TFIM. (a) and (b) show the m dependence of the eight lowest eigenvalues E_i and their absolute errors, $\delta E_i = E_i - E_i^{\mathrm{ex}}$, respectively. Six variational layers ($L = 6$) are used.

3. Test on NISQ computers

Here we present the technical details of the test for our concurrent quantum eigensolver on real NISQ computers by taking the three-spin TFIM with one ancilla as an example.

A variational calculation generally needs an ample depth of the circuit to represent a highly entangled quantum state. However, too many variational parameters may induce the so-called barren-plateau effect, undermining the optimization performance in NISQ computers. This implies that we should take a balanced strategy to optimize the number of variational parameters and their implementation errors. Since two-qubit gates have much lower fidelity than single-qubit gates in currently available quantum computing platforms, we modify the variational ansatz to use more single-qubit gates to lower the use of two-qubit gates.

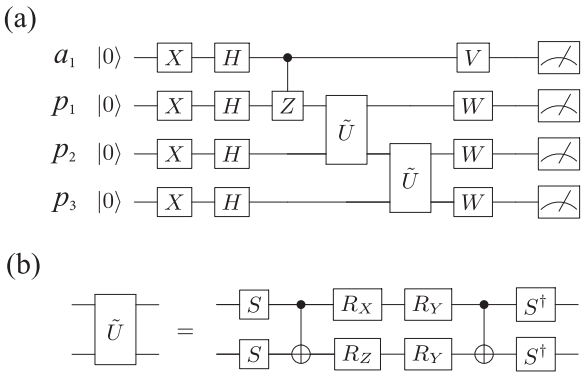

FIG. 6. (a) Variational circuit for solving the lowest two eigenenergies of the three-spin TFIM with one ancilla. $\tilde{U}$ is the two-qubit rotation gate, whose structure is depicted in (b). S is the phase gate, $S = R_Z(\pi/2)$.

Figure 6 shows the variational circuit used in our calculation. To improve the optimization process without increasing the number of two-qubit gates, we add additional single-qubit rotation gates along the Y axis between the two controlled-NOT (CNOT) gates, which introduces more variational parameters to improve the search capability of our ansatz. Note that there is no need to add the Z- and X-axis rotation gates because they commute with the CNOT gate, and these two kinds of gates are equivalent to rotating W gates.

We implemented our algorithm on the Oslo quantum processor on the IBM quantum computing platform. The result is shown in Fig. 3 of the main text. Our implementations use a full readout error-mitigation technique to determine the response matrix before the optimization. Applying this technique, we can mitigate the cross-talk effect [66,67] in the readout process. Given the small size of the circuit, this error-mitigation process is achievable with reasonable computational resources. Increasing the number of qubits, we can still mitigate the readout error under the assumption of an independent readout error model such as the tensor product noise model [68] using the bit-flip averaging technique [69].

[1] P. Shor, in *Proceedings of the 35th Annual Symposium on the Foundations of Computer Science* (IEEE Computer Society, Washington, DC, USA, 1994), pp. 124–134.

[2] S. Lloyd, Science **273**, 1073 (1996).

[3] A. W. Harrow, A. Hassidim, and S. Lloyd, Phys. Rev. Lett. **103**, 150502 (2009).

[4] L. K. Grover, in *Proceedings of the Twenty-Eighth Annual ACM Symposium on the Theory of Computing, STOC '96* (Association for Computing Machinery, New York, 1996), pp. 212–219

[5] D. P. DiVincenzo, Science **270**, 255 (1995).

[6] D. P. DiVincenzo, Fortschr. Phys. **48**, 771 (2000).

[7] A. Blais, A. L. Grimsmo, S. M. Girvin, and A. Wallraff, Rev. Mod. Phys. **93**, 025005 (2021).

[8] I. Bloch, J. Dalibard, and W. Zwerger, Rev. Mod. Phys. **80**, 885 (2008).

[9] C. Monroe, W. C. Campbell, L.-M. Duan, Z.-X. Gong, A. V. Gorshkov, P. W. Hess, R. Islam, K. Kim, N. M. Linke, G. Pagano, P. Richerme, C. Senko, and N. Y. Yao, Rev. Mod. Phys. **93**, 025001 (2021).

[10] P. Kok, W. J. Munro, K. Nemoto, T. C. Ralph, J. P. Dowling, and G. J. Milburn, Rev. Mod. Phys. **79**, 135 (2007).

[11] H. J. Mamin, M. Kim, M. H. Sherwood, C. T. Rettner, K. Ohno, D. D. Awschalom, and D. Rugar, Science **339**, 557 (2013).

[12] J. Preskill, Quantum **2**, 79 (2018).

[13] K. Bharti, A. Cervera-Lierta, T. H. Kyaw, T. Haug, S. Alperin-Lea, A. Anand, M. Degroote, H. Heimonen, J. S. Kottmann, T. Menke, W.-K. Mok, S. Sim, L.-C. Kwek, and A. Aspuru-Guzik, Rev. Mod. Phys. **94**, 015004 (2022).

[14] F. Arute, K. Arya, R. Babbush, D. Bacon, J. C. Bardin, R. Barends *et al.*, Nature (London) **574**, 505 (2019).

[15] H.-S. Zhong, H. Wang, Y.-H. Deng, M.-C. Chen, L.-C. Peng, Y.-H. Luo *et al.*, Science **370**, 1460 (2020).

[16] Y. Wu *et al.*, Phys. Rev. Lett. **127**, 180501 (2021).

[17] L. S. Madsen, F. Laudenbach, M. F. Askarani, F. Rortais, T. Vincent, J. F. F. Bulmer, F. M. Miatto, L. Neuhaus, L. G. Helt, M. J. Collins, A. E. Lita, T. Gerrits, S. W. Nam, V. D. Vaidya, M. Menotti, I. Dhand, Z. Vernon, N. Quesada, and J. Lavoie, Nature (London) **606**, 75 (2022).

[18] M. Cerezo, A. Sone, T. Volkoff, L. Cincio, and P. J. Coles, Nat. Commun. **12**, 1791 (2021).

[19] E. Farhi, J. Goldstone, and S. Gutmann, arXiv:1411.4028.

[20] M. C. Chen, M. Gong, X. Xu, X. Yuan, J.W. Wang, C. Wang, C. Ying, J. Lin, Y. Xu, Y. Wu, S. Wang, H. Deng, F. Liang, C. Z. Peng, S. C. Benjamin, X. Zhu, C. Y. Lu, and J. W. Pan, Phys. Rev. Lett. **125**, 180501 (2020).

[21] A. Peruzzo, J. McClean, P. Shadbolt, M.-H. Yung, X.-Q. Zhou, P. J. Love, A. Aspuru-Guzik, and J. L. O'Brien, Nat. Commun. **5**, 4213 (2014).

[22] J. I. Colless, V. V. Ramasesh, D. Dahlen, M. S. Blok, M. E. Kimchi-Schwartz, J. R. McClean, J. Carter, W. A. de Jong, and I. Siddiqi, Phys. Rev. X **8**, 011021 (2018).

[23] Y. Cao, J. Romero, J. P. Olson, M. Degroote, P. D. Johnson, M. Kieferová, I. D. Kivlichan, T. Menke, B. Peropadre, N. P. D. Sawaya, S. Sim, L. Veis, and A. Aspuru-Guzik, Chem. Rev. **119**, 10856 (2019).

[24] H. R. Grimsley, S. E. Economou, E. Barnes, and N. J. Mayhall, Nat. Commun. **10**, 3007 (2019).

[25] G. Harsha, T. Shiozaki, and G. E. Scuseria, J. Chem. Phys. **148**, 044107 (2018).

[26] S. McArdle, S. Endo, A. Aspuru-Guzik, S. C. Benjamin, and X. Yuan, Rev. Mod. Phys. **92**, 015003 (2020).

[27] A. G. Taube and R. J. Bartlett, Int. J. Quantum Chem. **106**, 3393 (2006).

[28] P. J. Ollitrault, A. Kandala, C.-F. Chen, P. K. Barkoutsos, A. Mezzacapo, M. Pistoia, S. Sheldon, S. Woerner, J. M. Gambetta, and I. Tavernelli, Phys. Rev. Res. **2**, 043140 (2020).

[29] J. Tilly, G. Jones, H. Chen, L. Wossnig, and E. Grant, Phys. Rev. A **102**, 062425 (2020).

[30] J. S. Kottmann, A. Anand, and A. Aspuru-Guzik, Chem. Sci. **12**, 3497 (2021).

[31] M. Benedetti, E. Lloyd, S. Sack, and M. Fiorentini, Quantum Sci. Technol. **4**, 043001 (2019).

[32] T. Kimura, K. Shiba, C.-C. Chen, M. Sogabe, K. Sakamoto, and T. Sogabe, Math. Probl. Eng. **2021**, e3511029.

[33] E. Grant, L. Wossnig, M. Ostaszewski, and M. Benedetti, Quantum **3**, 214 (2019).

[34] J.-G. Liu, L. Mao, P. Zhang, and L. Wang, Mach. Learn.: Sci. Technol. **2**, 025011 (2021).

[35] C. Bravo-Prieto, J. Lumbreras-Zarapico, L. Tagliacozzo, and J. I. Latorre, Quantum **4**, 272 (2020).

[36] C. Cade, L. Mineh, A. Montanaro, and S. Stanisic, Phys. Rev. B **102**, 235122 (2020).

[37] Z. Cai, Phys. Rev. Appl. **14**, 014059 (2020).

[38] J.-M. Reiner, F. Wilhelm-Mauch, G. Schön, and M. Marthaler, Quantum Sci. Technol. **4**, 035005 (2019).

[39] S. Yalouz, B. Senjean, F. Miatto, and V. Dunjko, Quantum **5**, 572 (2021).

[40] A. Uvarov, J. D. Biamonte, and D. Yudin, Phys. Rev. B **102**, 075104 (2020).

[41] J.-G. Liu, Y.-H. Zhang, Y. Wan, and L. Wang, Phys. Rev. Res. **1**, 023025 (2019).

[42] T. Jones, S. Endo, S. McArdle, X. Yuan, and S. C. Benjamin, Phys. Rev. A **99**, 062304 (2019).

[43] J. Tilly, H. Chen, S. Cao, D. Picozzi, K. Setia, Y. Li, E. Grant, L. Wossnig, I. Rungger, G. H. Booth, and J. Tennyson, Phys. Rep. **986**, 1 (2022).

[44] J. R. McClean, M. E. Kimchi-Schwartz, J. Carter, and W. A. de Jong, Phys. Rev. A **95**, 042308 (2017).

[45] O. Higgott, D. Wang, and S. Brierley, Quantum **3**, 156 (2019).

[46] J. Wen, D. Lv, M.-H. Yung, and G.-L. Long, Quantum Eng. **3**, e80 (2021).

[47] K. Kuroiwa and Y. O. Nakagawa, Phys. Rev. Res. **3**, 013197 (2021).

[48] K. M. Nakanishi, K. Mitarai, and K. Fujii, Phys. Rev. Res. **1**, 033062 (2019).

[49] R. M. Parrish, E. G. Hohenstein, P. L. McMahon, and T. J. Martínez, Phys. Rev. Lett. **122**, 230401 (2019).

[50] K. Mitarai, M. Negoro, M. Kitagawa, and K. Fujii, Phys. Rev. A **98**, 032309 (2018).

[51] M. Schuld, V. Bergholm, C. Gogolin, J. Izaac, and N. Killoran, Phys. Rev. A **99**, 032331 (2019).

[52] J. Schwinger, Phys. Rev. **128**, 2425 (1962).

[53] S. Coleman, Ann. Phys. (NY) **101**, 239 (1976).

[54] M. Bañuls, K. Cichy, J. Cirac, and K. Jansen, J. High Energ. Phys. 11 (2013) 158.

[55] F. Verstraete, J. J. García-Ripoll, and J. I. Cirac, Phys. Rev. Lett. **93**, 207204 (2004).

[56] M. Kleinmann, H. Kampermann, T. Meyer, and D. Bruß, Phys. Rev. A **73**, 062309 (2006).

[57] M. J. Gullans and D. A. Huse, Phys. Rev. X **10**, 041020 (2020).

[58] M. A. Nielsen and I. L. Chuang, *Quantum Computation and Quantum Information*, 10th ed. (Cambridge University Press, Cambridge, 2010).

[59] S. Endo, I. Kurata, and Y. O. Nakagawa, Phys. Rev. Res. **2**, 033281 (2020).

[60] S. Cao, L. Wossnig, B. Vlastakis, P. Leek, and E. Grant, Phys. Rev. A **101**, 052309 (2020).

[61] J. Wu and T. H. Hsieh, Phys. Rev. Lett. **123**, 220502 (2019).

[62] J. Zeng, C. Cao, C. Zhang, P. Xu, and B. Zeng, Quantum Sci. Technol. **6**, 045009 (2021).

[63] J. R. McClean, S. Boixo, V. N. Smelyanskiy, R. Babbush, and H. Neven, Nat. Commun. **9**, 4812 (2018).

[64] E. K. U. Gross, L. N. Oliveira, and W. Kohn, Phys. Rev. A **37**, 2805 (1988).

[65] D. Wecker, M. B. Hastings, and M. Troyer, Phys. Rev. A **92**, 042303 (2015).

[66] Y. Chen, M. Farahzad, S. Yoo, and T.-C. Wei, Phys. Rev. A **100**, 052315 (2019).

[67] J. Heinsoo, C. K. Andersen, A. Remm, S. Krinner, T. Walter, Y. Salathé, S. Gasparinetti, J.-C. Besse, A. Potočnik, A. Wallraff, and C. Eichler, Phys. Rev. Appl. **10**, 034040 (2018).

[68] S. Bravyi, S. Sheldon, A. Kandala, D. C. Mckay, and J. M. Gambetta, Phys. Rev. A **103**, 042605 (2021).

[69] A. W. R. Smith, K. E. Khosla, C. N. Self, and M. S. Kim, Sci. Adv. **7**, eabi8009 (2021).